A Low-Profile Wideband Dual-Sense Circularly Polarized MIMO Antenna for mmWave Applications

Shahid Ullah, Yejun He, *Senior Member, IEEE*, Abdul Majeed, and Yi Huang, *Fellow, IEEE*

***Abstract*—A wideband, dual-sense circularly polarized millimeter-wave multiple-input multiple-output (MIMO) antenna with a low profile is presented in this letter by using a tapered microstrip line, parasitic/meta-surface elements, and shared defected ground plane. The electrical footprint of the four-port MIMO antenna is 1.63λ× 1.63λ× 0.04λ, where λ is the free space wavelength at the lower operating frequency, and has a single-layered prototype manufactured on the Rogers 5880 substrate. The wide operating frequency bandwidth (17.5 GHz to 40 GHz) is achieved by the installation of a special meander line structure and tapered microstrip line. The isolation and axial ratio (AR) bandwidth are enhanced with the help of parasitic meta-surface elements and connected ground plane with circular shape defected ground structure. A good diversity performance with channel capacity loss of no more than 0.25, mean effective gain of no more than 1.05 dB, envelope correlation coefficient of no more than 0.025, diversity gain value of no less than 9.99 dB, and total active reflection coefficient of lower than −10 dB is achieved. The AR covers 5G bands of 24 GHz, 28 GHz, and 31 GHz.**

***Index Terms*—Axial ratio (AR), circularly polarized (CP), millimeter-wave (mmWave) technology, multiple-input multiple-output (MIMO) antenna, wide bandwidth.**

I. Introduction

CURRENTLY, the lower frequency microwave band has been already occupied, and there is a need for a high data rate, improved channel capacity, and high reliability for advanced wireless communication systems [1]. The new millimeter-wave (mmWave) frequency band (30 GHz to 300 GHz) is introduced in 5G new radio that has a demand for multigigabit/second data rate speed [2]. Different countries are using different frequency ranges for 5G mmWave applications.

The modern wireless communication system requires a multiple-input multiple-output (MIMO) antenna, wide bandwidth for high data rate, and circular polarization for reliable communication. However, fast wireless communication has multipath fading issues in dense areas, and the MIMO antenna is the solution that will enhance the channel capacity, spectral efficiency, and reliability of the communication system. The channel capacity is affected by the coupling between the antenna elements, and for the isolation improvement between antennas, different techniques have been presented in previous works, such as split ring resonator (SRR) [3], defected ground structure (DGS) [4], electronic band gap [5], parasitic elements [6], and metamaterial superstrate [7]. For a wide bandwidth MIMO antenna, a simple patch structure is not a good candidate because it has a narrow bandwidth. In the literature, multiple techniques have been used for wide bandwidth achievement, such as SRR base monopole antenna [8], slotted microstrip feeding [9], and semicircular monopole, by using a slot on the radiator and ground plane [4]. For MIMO antennas, every radiating element must have a common connected ground plane that will maintain a single reference voltage and achieve a high gain.

In mmWave technology, circularly polarized (CP) MIMO antennas play an important role in removing the mismatch loss between transmitter and receiver during the rotation of communication devices, which is not possible in linearly polarized (LP) antennas. The LP antennas radiate in one direction, whereas CP antennas radiate in two directions with the same magnitude [10]. Moreover, with the help of CP patterns, obstacle penetration is possible and that is why CP antennas are widely used for the enhancement of communication capacity, and effectiveness to resist multipath propagation. Nowadays, dual-polarized MIMO antennas are more attractive for research work. Several dual-band CP polarized antennas are discussed, such as an inverted L-shape dual-CP antenna [11], a CP MIMO antenna based on a dielectric resonator [12], and a series slot-fed MIMO antenna array is presented with CP diversity in [13]. The MIMO antennas have produced only left-hand CP (LHCP) or right-hand CP (RHCP) waves, as depicted in [14], whereas Sofi et al. [15] produced dual-CP waves, but their bandwidth of operating frequency and axial ratio (AR) are smaller and have multiple layers. There is a lack of work on the CP MIMO antennas in the mmWave frequency band used for 5G communication, and mostly, the MIMO antennas have wide bandwidth but do not have CP properties [16]. To the best of the authors' knowledge, none of the reported four-port of MIMO antennas in the literature simultaneously includes the performance of single layer, connected ground, wide bandwidth, dual circular polarization, high isolation, large AR bandwidth, and MIMO features at the range of mmWave band.

The main contributions of the letter are as follows. 1) Low-profile MIMO antenna with dual-sense property is obtained. We organize the four antennas with appropriate placement, which plays an important role in the compactness and dual-sense property of the MIMO antenna. 2) Wide operating impedance bandwidth is achieved due to the use of a meander line structure

Received 28 February 2025; revised 25 March 2025; accepted 31 March 2025. Date of publication 3 April 2025; date of current version 6 August 2025. This work was supported in part by the National Key Research and Development Program of China under Grant 2023YFE0107900; in part by the National Natural Science Foundation of China under Grant 62071306; and in part by the Shenzhen Science and Technology Program under Grant JCYJ 20241202124219023. *(Corresponding author: Yejun He.)*

Shahid Ullah, Yejun He, and Abdul Majeed are with the State Key Laboratory of Radio Frequency Heterogeneous Integration, Sino-British Antennas and Propagation Joint Laboratory of MOST, Guangdong Engineering Research Center of Base Station Antennas and Propagation, Shenzhen Key Laboratory of Antennas and Propagation, College of Electronics and Information Engineering, Shenzhen University, Shenzhen 518060, China (e-mail: Shahidkhan@szu.edu.cn; heyejun@126.com; abdul@szu.ed.cn).

Yi Huang is with the Department of Electrical Engineering and Electronics, University of Liverpool, L69 7ZX Liverpool, U.K. (e-mail: Yi.Huang@liverpool.ac.uk).

Digital Object Identifier 10.1109/LAWP.2025.3557572

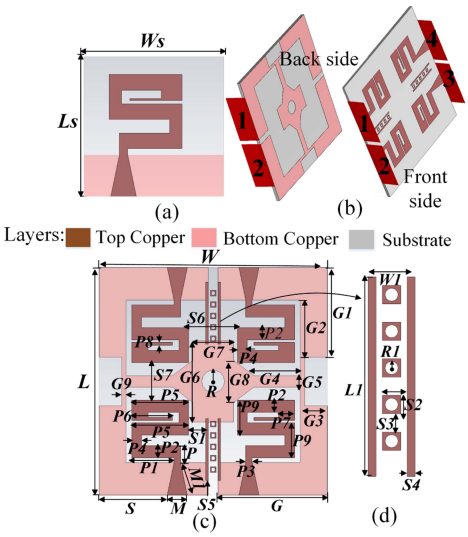

Fig. 1. (a) Structure of single meander line antenna. (b) 3-D (front and back side) view. (c) Detailed dimensions of the proposed four-port MIMO antenna. (d) Parasitic element.

TABLE I
DIMENSIONS OF THE PROPOSED MIMO ANTENNA

Parameter	Value (mm)	Parameter	Value (mm)	Parameter	Value (mm)
L=W	28	*P1=P6=G7*	5	*P7*	2
Ws=Ls=G	13.4	*P2*	1.5	*P8*	0.35
M	2.46	*P3*	0.8	*P9*	4.3
M1	4.09	*P4=W1*	1.2	*R*	1.4
P=S1	2.1	*P5=G2*	7	*R1*	0.25
S	8.37	*S2=S3*	0.7	*S4*	0.3
S5	1.5	*S6*	6	*S7*	4.6
G1	11	*G3*	3.3	*G4, G5*	5.7, 1.4
G6	10	*G8*	5.8	*G9, L1*	0.55, 7.63

and tapered microstrip line. 3) Three wide bandwidths of AR are obtained by using parasitic elements and shared DGS.

II. CP MIMO Antenna Design

A. Single Antenna Configuration and Operation

A single wide bandwidth antenna is designed using Roger RT5880 substrate with $\varepsilon_r = 2.2$, thickness of 0.787 mm, and loss tangent of 0.0009, and the total dimensions are $Ws \times Ls$, as shown in Fig. 1(a). Tapered microstrip 50 Ω feeding line is used for best matching and having low loss. An S-shaped stepped meander line radiating structure is used at the top side of the substrate, and at the bottom side a half ground plane is used to achieve a wider bandwidth. Every brick of the meander line has its separate operating frequency, and their dimensions are shown in Table I. The width and length of every brick and the space between the parallel bricks are optimized to achieve a wide bandwidth. The higher length lines are operating at the lower frequency, and smaller lengths are operating at the higher frequency. The single antenna simulated with the help of CST Microwave Studio 2022 operates at the frequency range of 14.1 GHz to 40 GHz, and two dual-band AR bandwidths (28.3 GHz to 29.5 GHz and 37.3 GHz to 38.8 GHz) are obtained, as shown in Fig. 2(a). As shown in Fig. 2(c), the gain and efficiency are 6 dBi and 95%, respectively.

B. Four-Port MIMO Antenna Configuration and Operations

The proposed MIMO is configured into four steps for the optimal value of isolation, small size, dual-sense CP properties, and wider AR bandwidth. The "3-D" view of the proposed

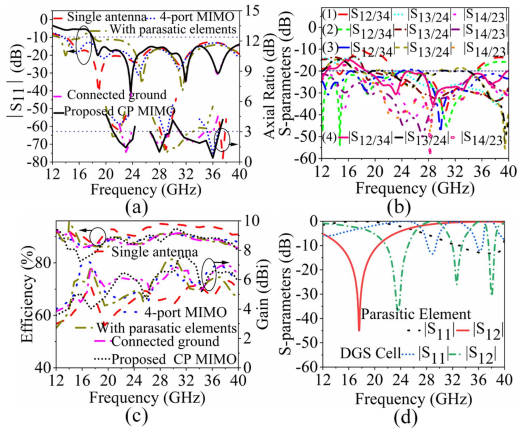

Fig. 2. Simulated (a) reflection coefficient (dB) and AR. (b) Transmission coefficient (dB) of four steps. (c) Efficiency (%) and gain (dBi) of the single antenna, and along with all four steps of MIMO antenna configuration. (d) S-parameters of a unit parasitic element and DGS cell.

MIMO antenna with four-port is shown in Fig. 1(b). In the first step, four-port elements are settled by placing two single mirror structure (S-shaped and Z-shaped) elements at a distance of $S6$, and both the pairs of the same element are placed identically along the x-axis by placing at the edge-to-edge distance of S7S7, as depicted in Fig. 1(c). The advantages of the element placement in the MIMO system are for miniaturization and dual-sense properties. The dimensions parameter values of the MIMO antenna are discussed in Table I. At this stage, the MIMO antenna operates at the frequency range of 13.8 GHz to 40 GHz, and its AR has too much narrow bandwidth (36.5 GHz to 37.3 GHz). The mutual coupling between two adjacent-port antenna is very high (≥ 10.2 dB), which affects the performance of the MIMO. The simulated reflection coefficient (dB) and AR (dB) of all steps are presented in Fig. 2(a), and isolation is presented in Fig. 2(b). The gain (dBi) and efficiency (%) of all the steps are presented in Fig. 2(c).

To solve the issue of isolation and improve AR bandwidth in the second step, a new parasitic element is placed among two adjacent radiating elements, as represented in Fig. 1(d). At this step, the antenna impedance operating frequency bands are 12.95 GHz to 16.1 GHz and 18.1 GHz to 40 GHz, and the AR bandwidth is enhanced, which is operating from 28.1 GHz to 31.3 GHz. It has a 7.5 dB isolation improvement at the required higher frequency. The simulated reflection coefficient and transmission coefficient of this element are presented in Fig. 2(d). It is used as a reflector between the antenna elements in the MIMO that can filter the lower operating frequency and have high isolation. Before adding these elements, the effect of coupling among the MIMO elements is substantive, but with these elements, it is decreased, as illustrated in Fig. 2(b). There is still a smaller coupling effect at the lower frequency that is removed in the next step with the connected ground plane. In the next step, a new structure is added to the ground of the MIMO that can help to increase the isolation and improve the bandwidth of AR for a good circular polarization, as illustrated in Fig. 2(a), with all the proposed dimensions. It has connected the ground plane of each element of the MIMO antenna with the intention of the same voltage flow during operation. Now, the operating frequency is from 17.9 GHz to 40 GHz, and the AR is operated at the triband (22.2 GHz to 23.5 GHz, 27 GHz to 29 GHz, and 30.5 GHz to 36 GHz), and isolation among the elements is better than 18.5 dB. To enhance the bandwidth of AR operating bands and isolation, a circular DGS structure is added into the ground

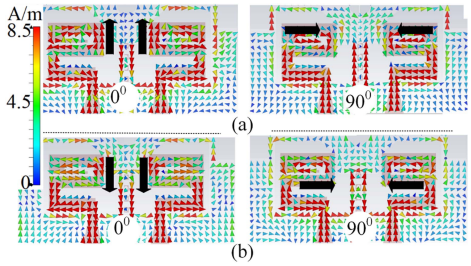

Fig. 3. Surface current distributions between two mirror structures at phase angles (0° and 90°) for (a) 24 GHz and (b) 28 GHz.

of the antenna with a radius of R, as illustrated in Fig. 1(a), and the S-parameter results of the cell are shown in Fig. 2(d). There is no change in the operating impedance frequency, but the AR operates at the three wide bandwidths of 2.2 GHz (21.9 GHz to 24.1 GHz), 2.12 GHz (26.9 GHz to 29.2 GHz), and 6.6 GHz (30.5 GHz to 37.1 GHz), and the isolation is below of 20 dB. The DGS slot can interrupt the uniform current distribution in the ground, and as a result, the antenna has better CP properties. The current MIMO antenna has a simulated gain of 7.61 dBi and has 93% radiating efficiency.

The current direction of the elements (S-shaped and Z-shaped) is opposite and has the same magnitude, which proves the properties of a dual-CP antenna. Due to the dual-polarized property of the proposed meander line antenna, the current flow changes at different operating frequencies. At the lower frequency of 24 GHz, the Z-shaped radiator has a clockwise while S-shaped has anticlockwise current flow at both angles ($\phi = 0°$ and 90°) of variation, as depicted in Fig. 3(a). However, at the high frequency of 28 GHz, the Z-shaped is anticlockwise while the S-shaped is clockwise current flow, as depicted in Fig. 3(b). Thus, the Z-shaped line has a property of LHCP at 24 GHz but RHCP at 28 GHz. Also, the S-shaped line is RHCP at 24 GHz but LHCP at 28 GHz. So, the proposed MIMO shows a dual CP property.

III. Experimental, Numerical Results, and Discussion of CP MIMO Antenna

A. S-Parameters, AR, Gain, and Efficiency

The presented MIMO antenna is fabricated and tested with the help of a vector network analyzer (VNA) and high-frequency mmWave anechoic chamber. The front and backside views of the prototype are shown in Fig. 4(a). The comparison of the simulated and measured reflection coefficient is depicted in Fig. 4(b), where all the ports are measured with the help of VNA, but at the same time only two ports can be measured, and the other two are connected with 50 Ω load connectors. It is detected that the measured results agree with the simulated results and cover the wide bandwidth (17.5 GHz to 40 GHz) of the mmWave band. The antenna is highly sensitive, and the small difference occurs due to the fabrication and soldering of the special connector. The AR and gain are tested at the peak radiation direction (theta=0°), where the measured AR is operating at the frequency bands of 21.5 GHz to 24.05GHz, 27 GHz to 29.7GHz, and 30.9 GHz to 36.9 GHz, as shown in Fig. 4(b). The AR results of all the ports are the same, so only a single port result is presented. The isolation performance of the four-port MIMO antenna is characterized by the help of S-parameters where the simulated and measured results have greater than 20 dB isolation, as depicted in Fig. 4(c). The proposed CP MIMO antenna gain and efficiency are depicted

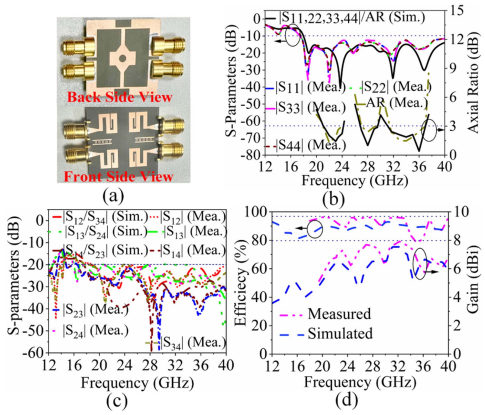

Fig. 4. Simulated and measured (a) reflection coefficient (dB) and AR (dB), (b) transmission coefficient (dB) of four ports, as well as (c) gain (dBi), and radiation efficiency (%).

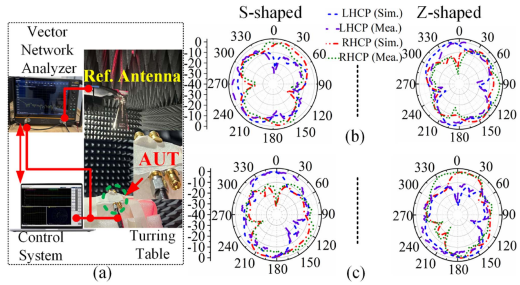

Fig. 5. (a) Measurement setup of anechoic chamber. The simulated and measured radiation patterns at operating frequencies of (b) 24 GHz and (c) 28 GHz.

in Fig. 4(d). The maximum measured gain and efficiency at the operating band are 8 dBi and 96%, respectively.

B. Radiation Patterns

The Anechoic chamber testing setup for the proposed MIMO antenna is illustrated in Fig. 5(a). In a chamber, only one port can be measured at a time, whether in port 1 (Z-shaped) or port 2 (S-shaped) structure. The patterns are generated at a single plane with the orientation of 90° ("Phi" angle) to find the polarization properties of both shapes used in the CP MIMO. It shows that both of the shape's polarization characteristics (LHCP and RHCP) are switched to each other, but there is no variation in the magnitude. The S-shaped elements have RHCP polarization behavior, and the Z-shaped elements have LHCP behavior at operating frequencies of 24 GHz, as depicted in Fig. 5(b). In the main lobe of the S-shaped, the RHCP radiation surpassed LHCP, whereas the Z-shaped LHCP surpassed RHCP by a difference of more than 20 dB. At 28 GHz, the behavior of the CP property is changed, as depicted in Fig. 5(c). The S-shaped elements have LHCP polarization behavior, and the Z-shaped elements have RHCP behavior. Thus, it is evident that this CP MIMO antenna exhibits both RHCP and LHCP characteristics.

C. Diversity Performance

The diversity performance of the MIMO antennas is very important to describe the standard isolation of the MIMO. The diversity parameters consist of total active reflection coefficient (TARC), channel capacity loss (CCL), envelope correlation coefficient (ECC), diversity gain (DG), and mean effective gain

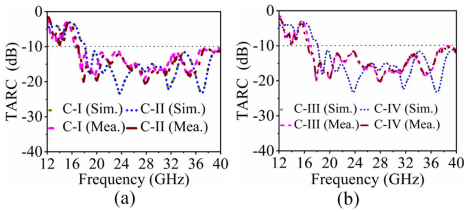

Fig. 6. Different cases (C-.) of simulated and measured TARC. (a) C-I ($\theta_1 = 30$, $\theta_2 = 60$, and $\theta_3 = 90$) and C-II ($\theta_1 = 60$, $\theta_2 = 90$, and $\theta_3 = 120$). (b) C-III ($\theta_1 = 45$, $\theta_2 = 90$, and $\theta_3 = 135$) and C-IV ($\theta_1 = 90$, $\theta_2 = 135$, and $\theta_3 = 180$).

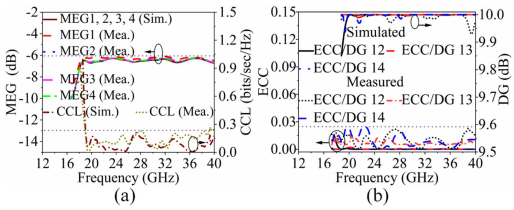

Fig. 7. (a) CCL (bit/s/Hz), and MEG plots, as well as (b) ECC and DG (dB) of the proposed MIMO antenna.

(MEG). The meaning of the TARC is the same as that of the single antenna reflection coefficient that considers the overall MIMO elements reflection coefficient. It is important for the effective bandwidth determination and to define the radiation performance of the MIMO. The proposed four-port CP MIMO uses the equation as mentioned in [17] to calculate the diversity parameters. TARC values can be calculated by using the input signal at different angle excitation. The input signal phase at the first element is e^{j0} (reference phase), while the other elements receive different phase excitations. In the current work, four different cases (C-I, II, III, and IV) are discussed to evaluate the TARC values by changing phase differences. Fig. 6(a) and (b) indicates that cases one (C-I) and two (C-II) have a difference of 30°, whereas cases three (C-III) and four (C-IV) have a difference of 45°. These results show that the values are below −10 dB in the mentioned operating band.

The next important metric is CCL, which describes the highest standard threshold value of the transmission loss in transfer with a high data rate at which the signal can be safely transmitted throughout the operating band with less than 0.4 bit/s/Hz loss value. The calculated value of the proposed simulated and measured MIMO antenna is less than 0.25 bit/s/Hz throughout the operating wide band, as depicted in Fig. 7(a).

The gain of the MIMO antenna is analyzed by the diversity parameter known as MEG. For multiple antenna elements (port i and port j), it is calculated with the help of the four-port MEG equation. The values of the simulated MEG in this work are less than −6.2 dB, and the measured values are less than −6.15, as illustrated in Fig. 7(b), while the acceptable value of MEG should be less than −3 dB [17].

The ECC is an important parameter to calculate the correlation between the MIMO antenna elements. In practice, the value should be less than 0.5, which shows that there is a low correlation between MIMO antenna elements. The accurate method of ECC calculation uses far-field radiation patterns rather than *S*-parameters [10]. The calculated ECC is illustrated in Fig. 7(c), where a maximum of 0.0026 value is depicted throughout the operating simulated frequency band, and the measured ECC value is up to 0.025, which is too much less than the acceptable value.

The DG has a link with ECC, which is described in [10]. When the ECC values decrease, then the DG values are near 10 dB. In the MIMO antenna, the values of DG are greater than 9.99 dB at the operating frequency band, as illustrated in Fig. 7(c).

TABLE II
COMPARISON OF THE PROPOSED MIMO ANTENNA WITH EXISTING WORKS

Ref. Number	[15]	[18]	[19]	[20]	This Work
Size (λ^3)	1.5 ×2.92 ×2.92	2.9 ×1.8 ×0.04	4.3 ×1.7 ×0.03	1.5 ×1.86 ×0.04	1.63 ×1.63 ×0.04
Number of ports	4	2	8	4	4
Bandwidth (%)	16.8, 2.5	26.9	58	5.6, 18.42	78.2
Polarization	LHCP, RHCP	LHCP, RHCP	LHCP	LHCP	LHCP, RHCP
AR (%)	11.5, 3.69	2.9, 4.1	16.6, 10.5, 16.2	3.2, 1.65	11.2, 9.5, 17.7
CP Techniques	Using polarization converter	Slots in circular patch and ground	Metamaterial inspired elements	Characteristic mode analysis (CMA)	Meandered Design
Isolation (dB)	≥ 19	≥ 20	≥ 20	≥ 20	≥ 20
Radiation efficiency(%)	95	–	75	94	96
Gain (dBi)	5.75	6	20.5	12.69	8
ECC/ DG (dB)	≤ 0.15/ ≥ 9.99	≤ 0.003/ ≥ 9.9	≤ 0.005/ ≥ 9.99	–	≤ 0.025/ ≥ 9.99
MEG (dB)/ CCL (bps/Hz)	–	≤ −6/ ≤ 0.26	≤ −3.2/–	–	≤ −6.15/ ≤ 0.25

IV. COMPARISON

Table II explains the comparison of the proposed MIMO antenna with the previous wide bandwidth single and dual-sense CP MIMO antennas used for 5G applications. In the literature, there are a few wide bandwidth MIMO antennas with dual-sense CP properties and mostly have wide operating bandwidth but no CP property. In contrast to other wide bandwidth mmWave MIMO antennas, this one is nearly small in size and constructed on a less expensive substrate, making it cheaper for the mmWave spectrum. It is presented in [19] that the MIMO antenna has wide operating bandwidth with CP properties and has three AR bands, but it has eight ports, no dual-sense CP properties, and a large size. In comparison, the measured results of this work presented a wide bandwidth of operating frequency, miniaturized size, and three AR-wide operating bands covering the key mmWave bands.

V. CONCLUSION

This letter presented a new structure of the meander line, which has properties of mutual coupling for wide bandwidth achievement. A tapered microstrip line is used for best matching, and a new parasitic element is presented for high isolation. It uses shared ground with the defective ground via a single hole to provide dual CP characteristics with a wide range of ARs. A prototype of this CP MIMO antenna is fabricated and measured. The three important mmWave bands are covered by this MIMO antenna with measured AR (dB) at the central frequency of 24 GHz, 28 GHz, and 36 GHz. It has a wide relative operating frequency bandwidth of 78.2 %, which will replace the use of multiple antennas by using only a single MIMO antenna. The performance of TARC, DG, ECC, MEG, and CCL is highly acceptable as compared to the corresponding standard values. Due to the shared ground, single-layered, wide AR bandwidth, as well as high isolation, the presented MIMO antenna is a good candidate for mmWave wireless communication system.

REFERENCES

[1] R. G. Vaughan and J. B. Andersen, "Antenna diversity in mobile communications," *IEEE Trans. Veh. Technol.*, vol. VT-36, no. 4, pp. 149–172, Nov. 1987.

[2] S. Kim et al., "Coexistence of 5G with the incumbents in the 28 and 70 GHz bands," *IEEE J. Sel. Areas Commun.*, vol. 35, no. 6, pp. 1254–1268, Jun. 2017.

[3] A. Ramachandran, S. Mathew, V. Rajan, and V. Kesavath, "A compact triband quad-element MIMO antenna using SRR ring for high isolation," *IEEE Antennas Wireless Propag. Lett.*, vol. 16, pp. 1409–1412, 2017.

[4] P. Kumar et al., "A compact quad-port UWB MIMO antenna with improved isolation using a novel mesh-like decoupling structure and unique DGS," *IEEE Trans. Circuits Syst. II, Exp. Briefs*, vol. 70, no. 3, pp. 949–953, Mar. 2023.

[5] M. Alibakhshikenari et al., "Study on isolation improvement between closely-packed patch antenna arrays based on fractal metamaterial electromagnetic bandgap structures," IET *Microw., Antennas Propag.*, vol. 12, no. 14, pp. 2241–2247, Oct. 2018.

[6] J. Kulkarni, C.-Y.-D. Sim, B. Garner, and Y. Li, "A dual CP quad-port MIMO antenna with reduced mutual coupling for X-band application," *IEEE Antennas Wireless Propag. Lett.*, vol. 22, no. 9, pp. 2085–2089, Sep. 2023.

[7] I. Khan, K. Zhang, L. Ali, and Q. Wu, "Enhanced quad-port MIMO antenna isolation with metamaterial superstrate," *IEEE Antennas Wireless Propag. Lett.*, vol. 23, no. 1, pp. 439–443, Jan. 2024.

[8] R. Anitha, P. V. Vinesh, K. C. Prakash, P. Mohanan, and K. Vasudevan, "A compact quad element slotted ground wideband antenna for MIMO applications," *IEEE Trans. Antennas Propag.*, vol. 64, no. 10, pp. 4550–4553, Oct. 2016.

[9] M. Sonkki, D. Pfeil, V. Hovinen, and K. R. Dandekar, "Wideband planar four-element linear antenna array," *IEEE Antennas Wireless Propag. Lett.*, vol. 13, pp. 1663–1666, Aug. 2014.

[10] M. H. Reddy, D. Sheela, and A. Swaminath, "A four port circularly polarized printed multiple-input multiple-output antenna with enhanced isolation," *Int. J. Commun. Syst.*, vol. 35, no. 4, Mar. 2022, Art. no. e5061.

[11] Chandu D. S., and S. S. Karthikeyan, "A novel broadband dual circularly polarized microstrip-fed monopole antenna," *IEEE Trans. Antennas Propag.*, vol. 65, no. 3, pp. 1410–1415, Mar. 2017.

[12] G. Bharti et al., "Two-port dual-band circularly polarized dielectric resonator-based MIMO antenna with polarization diversity," *Electromagnetics*, vol. 40, no. 7, pp. 463–478, Sep. 2020.

[13] U. Ullah, M. Al-Hasan, S. Koziel, and I. B. Mabrouk, "Series-slot-fed circularly polarized multiple-input–multiple-output antenna array enabling circular polarization diversity for 5G 28 GHz indoor applications," *IEEE Trans. Antennas Propag.*, vol. 69, no. 9, pp. 5607–5616, Sep. 2021.

[14] W. Li, K. W. Leung, and N. Yang, "Omnidirectional dielectric resonator antenna with a planar feed for circular polarization diversity design," *IEEE Trans. Antennas Propag.*, vol. 66, no. 3, pp. 1189–1197, Mar. 2018.

[15] M. A. Sofi, K. Saurav, and S. K. Koul, "Four-port orthogonal circularly polarized dual-band MIMO antenna with polarization and spatial diversity using a dual-band linear-to-circular polarization converter," *IEEE Trans. Antennas Propag.*, vol. 70, no. 9, pp. 8554–8559, Sep. 2022.

[16] A. Patel et al., "UWB CPW fed 4-port connected ground MIMO antenna for sub-millimeter-wave 5G applications," *Alexandria Eng. J.*, vol. 61, no. 9, pp. 6645–6658, Sep. 2022.

[17] B. Aghoutane et al., "A novel dual-and high gain 4-port millimeter wave MIMO antenna array for 28/37 GHz 5G applications," *AEU- Int. J. Electron. Commun.*, vol. 145, Feb. 2022, Art. no. 154071.

[18] R. N. Tiwari, V. Kaim, P. Singh, T. Khan, and B. K. Kanaujia, "Semi-flexible diversified circularly polarized millimeter-wave MIMO antenna for wearable biotechnologies," *IEEE Trans. Antennas Propag.*, vol. 71, no. 5, pp. 3968–3982, May 2023.

[19] A. Khan, Y. He, and Z. Chen, "An eight-port circularly polarized wideband MIMO antenna based on a metamaterial-inspired element for 5G mmWave applications," *IEEE Antennas Wireless Propag. Lett.*, vol. 22, no. 7, pp. 1572–1576, Jul. 2023.

[20] S. Sadeghi-Marasht, M. S. Sharawi, and A. Zhu, "Dual-band circularly polarized antenna array for 5G millimeter-wave applications," *IEEE Open J. Antennas Propag.*, vol. 3, pp. 314–323, Mar. 2022.